Fate of river-derived microplastics from the South China Sea: Sources to surrounding seas, shores, and abysses

Matsushita, Kosei
Uchiyama, Yusuke
Takaura, Naru
Kosako, Taichi

(Citation)
Environmental Pollution,308:119631

(Issue Date)
2022-09-01

(Resource Type)
journal article

(Version)
Accepted Manuscript

Fate of river-derived microplastics from the South China Sea: Sources to surrounding seas, shores, and abysses

Kosei Matsushita[1], Yusuke Uchiyama[1,2 a], Naru Takaura[3], and Taichi Kosako[2]

1. Department of Civil Engineering, Kobe University, Kobe, Japan
2. Coastal and Estuarine Environmental Department, Port and Airport Research Institute, Yokosuka, Japan
3. Tokyo Electric Power Company Holdings, Inc., Tokyo, Japan
a. Corresponding author: uchiyama@harbor.kobe-u.ac.jp

Abstract

Microplastics (MPs) in the ocean have been widely recognized as causing global marine environmental problems. To gain a quantitative and comprehensive understanding of oceanic MP contamination, detailed numerical Lagrangian particle tracking experiments were conducted to evaluate the regional oceanic transport and dispersal of MPs in the South China Sea (SCS) derived from three major rivers, Pearl (China), Mekong (Vietnam), and Pasig (the Philippines), which are known to discharge large amounts of plastic waste into the SCS. As previous field surveys have suggested, MP contamination spreads from the surface to the deeper ocean in the water column, we considered three types of MPs: (1) positively buoyant (light) MPs, (2) positively buoyant (light) MPs with random walk diffusion, and (3) full 3-D tracking of non-buoyant MPs that are passively transported by ambient currents. Transport patterns of these MPs from the three rivers clearly showed the intra-annual variability associated with seasonally varying circulations driven by the Asian monsoons in the SCS. Many MPs floating during the prevailing southwest monsoon are transported to the northwest Pacific Ocean and the East China Sea through the Luzon Strait and the Taiwan Strait to form MP *hotspots*. Non-buoyant MPs are broadly transported from the surface layer to depths of approximately 100 m or deeper, where in situ observations are rare. In addition, the buoyant MPs drifting on the continental shelf originating from southern China tend to be pushed toward the shore and beached by northward wind-induced currents more pronouncedly than the non-buoyant MPs. Therefore, the river-derived MPs to the SCS were found to serve as sources to adjacent basins and oceans, to be distributed not only in the upper layer but also in the abyssal ocean (non-buoyant MPs), and to be transported to the shores (buoyant MPs).

Keywords: river-derived microplastics; oceanic transport and dispersal; the South China Sea; Lagrangian particle tracking model; ROMS

1. Introduction

In recent years, marine plastic pollution has been widely recognized as one of the most important global environmental issues. Microplastics (MPs), which are plastic fragments degraded into a diameter of 5 mm or less, flow mainly from land into the ocean and drift for a long time. Because plastics readily adsorb chemical substances (Mato et al., 2001) and are accidentally ingested by zooplankton (Sun et al., 2017), and marine organisms (Zhu et al., 2019a), MPs may have a significant impact on our ecosystems. The annual plastic waste input to the ocean has been reported to be 4.8 to 12.7 million tons from 192 coastal countries (Jambeck et al., 2015). Among others, many major rivers in Asia are the largest sources of marine plastic discharge to the ocean, which account for approximately 67% of global river discharges of plastic waste (Lebreton et al., 2018). In addition, the recent study by Meijer et al. (2021) evaluated that more than 1,000 rivers account for 80 % of global annual emissions, which range between 0.8 million and 2.7 million tons per year, with small urban rivers among the most polluting. Field sampling of MPs found that East Asian seas have one of the highest contaminations in the world (Isobe et al., 2015), indicating that Asian-origin MPs have a significant influence on the distribution of marine MPs in the surrounding seas. To compromise a limited number of laborious and costly field observations on measuring plastic wastes in a vast expanse of oceans, numerical modeling studies have been conducted for the Japan Sea (Iwasaki et al., 2017) and the East China Sea (ECS; Zhang et al., 2020). The transport processes of MPs have thus been gradually clarified in these seas through numerical analyses. However, there are few modeling studies on MP transport for the South China Sea (SCS, **Figure 1**), although many emission sources exist in the region; the SCS is fringed by three countries in the top 20 plastic emitting countries to ocean, *viz*., the Philippines (1st), China (4th), and Vietnam (8th). In particular, the Philippines has 19 rivers out of the top 50 plastic emitting rivers (Meijer et al., 2021). Hence, the quantitative contribution of the rivers as the major plastic sources in the SCS to plastic pollution in and around the SCS is an important scientific question to be answered.

The SCS is the world's largest marginal sea located on the west coast of the Pacific Ocean (**Figure 1**). The six coastal SCS countries annually contribute 6.1×10^5 tons of the plastic waste, among which the Philippines, China, and Vietnam emit 3.6×10^5, 7.1×10^4, 2.8×10^4 (ton/y), respectively (Meijer et al., 2021). The Pasig River (the Philippines), the Pearl River (China), and the Mekong River (Vietnam), all of which have river mouths in the shore of the SCS, discharge 39,000, 110,000, and 23,000 tons of plastic waste into the ocean annually, ranking 8th, 3rd, and 11th, in the world, respectively (Lebreton et al., 2018). The most recent evaluation (Meijer et al., 2021) updated this ranking that the Pasig River may be the world’s largest plastic emitter. I Indeed, MP pollution has been found in the estuaries of these rivers (Emmerick et al., 2020; Lam et al., 2020). In particular, high concentrations of MP pollution were found in the coastal areas of southern China owing to the influence of the Pearl River-derived MPs (Cai et al., 2018; Lam et al., 2020). In contrast, MP pollution in the central SCS is not as severe as that in MP hotspots such as the coastal SCS (Cai et al., 2018), the ECS (Zhang et al., 2020), and the Japan Sea (Isobe et al., 2015). Therefore, it is necessary to accurately evaluate the

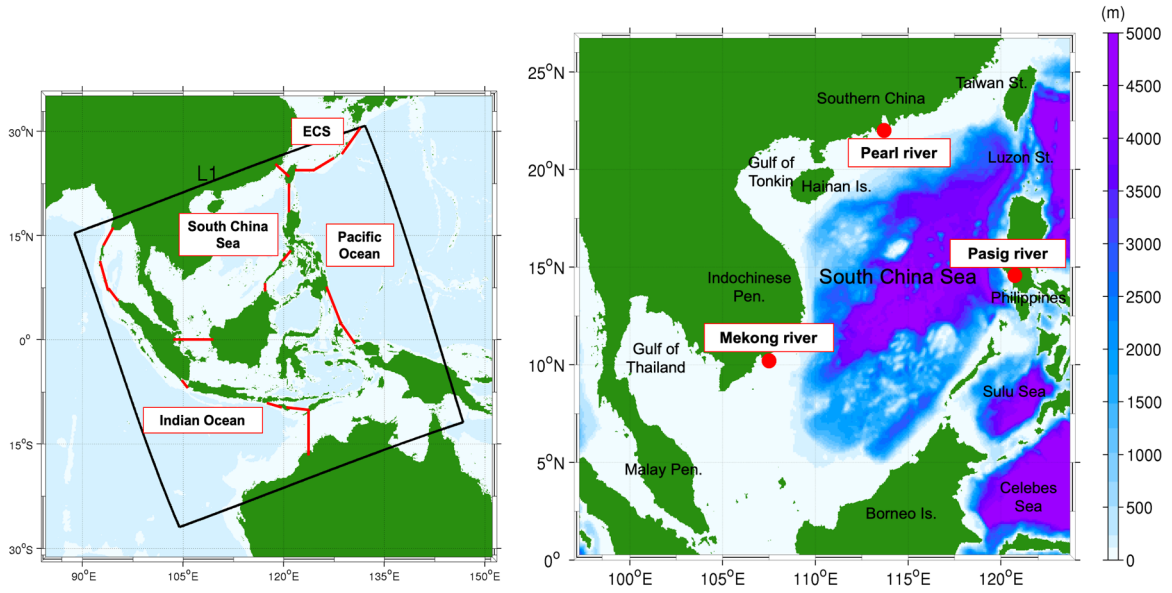

Figure 1. Left: Study area around the South China Sea. Red lines are the borders that separate the East China Sea (ECS), Pacific Ocean, Indian Ocean from the South China Sea. The black box corresponds to the HYCOM-ROMS model domain. Right: Enlarged view of the left panel with the locations of the four MPs release patches located at the mouths of the Pearl (China), Mekong (Vietnam), and Pasig (Philippines) rivers depicted by red circle marks. Colors show the bathymetry in meter.

transport processes of MPs derived from major rivers in the SCS and their possible remote influences on the surrounding seas, while it remains a challenge to compare MP pollution in the world's rivers due to the lack of standardized sampling and analytical protocols (Mai et al., 2019).

Most buoyant MPs are reported to exist within 1 m of the ocean surface (Reisser et al., 2015). They are also vertically distributed (Van Sebille et al., 2020) by vertical eddy mixing, which is enhanced in the surface boundary layer (Kukulka et al., 2012). As time progresses, the density of MPs may be altered owing to fragmentation, refinement, and biofouling (Kaiser et al., 2017; Fazey et al., 2016). Further degradation of MPs results in much finer, nanometer-sized pieces of plastic (Piccardo et al., 2020). Smaller plastic fragments have a larger surface area relative to their volume, promoting surface adhesion that increases the MP density, and thus is less likely to have an upward surfacing velocity (Chubarenko et al., 2016; Poulain et al., 2019). Accordingly, once MPs disappear from the ocean surface, they seldom return to the surface, and thus can be found in the ocean interior below the surface layer (Kooi et al., 2017). In fact, MPs have occasionally been observed in the deep ocean at depths ranging from several hundred meters to several thousand meters (Li et al., 2020). Zhu et al. (2019a) reported that all deep-sea fish collected from depths of 200–209 m and 453–478 m were contaminated by microplastics on the northern continental slope of the SCS. Isobe et al. (2019) succeeded in reproducing surface MP contamination in the Pacific Ocean with their horizontal two-dimensional (2DH) surface MP transport model if they introduced an *ad hoc* sink term crudely activated three years after MP is released to mimic downward MP transport. Cai et al. (2018) estimated that the top 5 m of the SCS contained around 700 tons of plastics; this is the current best available estimate of plastic mass present in SCS surface waters. However, they also pointed out that the MPs found in the surface ocean are one

to four orders of magnitude smaller than the reported emission, implying both a deficiency of sparse observations and the importance of non-buoyant plastics. Thus, it is profoundly important to scientifically understand the transport processes of MPs that are not only drifting in the surface layer, but also being passively transported by ambient currents in the interior ocean where observations of MPs have not yet been abundant.

In the present study, we aimed to answer the question on the fate of MPs derived from major rivers in the SCS by using a state-of-the-art three-dimensional (3D) ocean modeling technique coupled with an offline Lagrangian particle tracking model. As argued above, anticipated possible destinations include shallow coastal areas on the continental shelf of the SCS, the surface ocean in the middle of the SCS, the subsurface or abyssal ocean of the SCS, and the surrounding seas such as the ECS. Because transport and dispersal processes of MPs may differ according to their relative density to the seawater; two types of MPs, viz. positively buoyant (light) and neutrally buoyant (passive) MPs, were considered. Hence, we evaluated the 3D oceanic transport of MPs derived from three major rivers in the SCS, that is, Pearl (China), Mekong (Vietnam), and Pasig (the Philippines) rivers, as major sources of terrestrial plastic waste into the SCS. We investigated the horizontal transport patterns of MPs in and around the SCS along with possible driving mechanisms, and quantified the rate of MPs originating from the SCS that flowed out to the surrounding seas. Based on the modeled outcomes, we further discuss the possible impacts of high MP concentrations on MP pollution in East Asian seas and the differences in transport patterns of MPs of two different weight densities.

2. Methods

We conducted particle tracking experiments for both buoyant MPs and neutrally buoyant (non-buoyant) MPs driven by a pre-computed 3D Eulerian current velocity. To accurately evaluate the full 3D transport of MPs with different bulk densities accurately, a detailed three-dimensional flow field was evaluated using a high-precision hydrodynamic model that is capable of precisely reproducing the fully 3D oceanic flow from the surface to the ocean floor. Therefore, for a more precise determination of MP transport through narrow straits, around complex lateral topographies near the land, and islands under the influence of eddies; a higher grid resolution model is required. Accordingly, we utilized the HYCOM-ROMS downscaling model (Uchiyama et al. 2018c; 2019), which is a high-resolution eddy-resolving circulation model based on the Regional Oceanic Modeling System (ROMS; Shchepetkin and McWilliams, 2005; 2009) embedded in a HYCOM global reanalysis in an offline-nesting configuration (Mason et al., 2010; Uchiyama et al., 2014, 2017a, 2017b, 2018a, 2018b, 2022; Kamidaira et al., 2017, 2018, 2019, 2021; Kurosawa et al., 2020; Tada et al., 2018; Takeda et al., 2021; Zhang et al., 2019) with tides (Buijsman et al., 2012; Dauhajre et al., 2017; Masunaga et al., 2018, 2019). The model encompasses an extensive area as shown in **Figure 1**, and a numerical reanalysis was performed for a five-year period from 2011 to 2015, avoiding the medium-term climatology mode mainly due to ENSO (**Table 1a)**. More details of the HYCOM-ROMS model can be found in **Section S1** of **Supplemental Material.**

Table 1. Configurations of (a) HYCOM-ROMS ocean circulation model, (b) Lagrangian particle tracking experiment for three cases, and (c) mouth conditions of the three major rivers defined in the particle tracking model.

(a)

HYCOM-ROMS model configurations	
Computational period	1/16/2011–12/31/2015
Grid cells	1024 × 1024 × vertical 40 *s*-layers
Horizonal grid resolution	5 km
Baroclinic time step	60 s
Surface wind stress	GPV-GSM
Surface flux	NOAA-COADS (monthly climatology)
SST and SSS to restore	HYCOM (20-day averaged)
Open boundary/initial conditions	HYCOM (daily)
TS nudging	HYCOM (10-day averaged)
Tides	TPXO 7.0
Topography	SIO SRTM30_Plus

(b)

case	1. Buoyant (3D)	2. Buoyant (Surface2D + Random walk)	3. Passive
Rising velocity, w_{MP}	2 mm/s	–	–
Release depth	0.5m	–	0.5m
Number of patches		3	
Radius of patches		25 km	
Release period		1/1/2012-12/31/2014	
Release interval		12 hours	
Release time		2192	

(c)

River	Country	Longitude	Latitude	Released particles at each time	Total number of particles
Mekong	Vietnam	107.50°	10.20°	214	1,407,264
Pearl	China	113.70°	22.05°	210	1,380,960
Pasig	Philippine	120.75°	14.50°	172	1,131,072

We exploited the offline 3-D Lagrangian particle tracking model originally developed by Carr et al. (2008), forced by the HYCOM-ROMS model outputs, following the methodology described by Mitarai et al. (2009), Romero et al. (2013), and Uchiyama et al. (2018b) with several modifications (See **Sections S2** and **S3** of **Supplemental Material**). To investigate the effects of MP density on the dispersal processes, particle tracking experiments were conducted for three cases, viz., Case 1: buoyant MPs forced by the 3D currents, Case 2: buoyant MPs forced by the surface 2DH currents and placed in the top-most surface layer, and Case 3: non-buoyant MPs that are fully transported passively by the 3D currents (**Table 1b**). We presume that MPs are slightly buoyant to park in the near-surface layer and thus are not to be transported directly by windage for Cases 1 and 2, while Case 3 accounts for small-sized MPs that are neutrally buoyant with the rising velocity of $w_{MP} = 0$. The particles were released periodically at an interval of 12 hours from circular patches placed at the river mouths of interest (**Table 1b-c**). The radius of the circular patch was set to 25 km, in which particles were evenly placed to complement the under-resolved initial near-field dilution of MPs around river mouths. More than four million particles were released over the three years.

To determine the destination of MPs initially released from major rivers in the SCS, the beaching of MPs is considered in Cases 1 and 3. In this study, the MPs reaching a grid cell with the representative shallow water depth of 20 m, which pre-defined the minimum depth set in the HYCOM-ROMS model, are automatically deemed "beached." If the particle is judged as beached, the tracking is terminated, and the particle stops at this position. Case 2 is an exception to this protocol because of the inclusion of the random walk model, in which MPs that drifted onto the shore grid must be allowed to return to the ocean grid by forced horizontal MP displacement by the horizontal random walk. However, even for Case 2, the MPs reaching the shore grid are much less mobile as they spontaneously slow down according to the subgrid velocity interpolation towards zero velocity on the land grids. Moreover, we did not include the Stokes drift velocity (Uchiyama et al., 2010; 2017a) in the present study as argues in **Section S2**, except for the additional experimental run shown in **Section S4**.

3. Medium-term Oceanic Transport of MPs in and around the SCS

3.1 Mean seasonal hydrodynamic variability

As reviewed by Hu et al. (2000) and references therein, overall seasonal circulation in the SCS is cyclonic in winter and anticyclonic in summer with a few stable eddies, mostly driven by monsoon winds. These surface circulations are formed as intensive western boundary currents that extend to a depth of around 200 m (summer) to 500 m (winter) (Chu et al., 1999). The seasonal circulation is also affected by water exchange between the SCS and the adjacent seas. For instance, observational studies (e.g., Wyrtki, 1961; Song, 2006; Fang et al., 2010) show that there is volume outflow from the southern SCS into the Java Sea during winter and vice versa in summer, which have been confirmed by modeling studies (Cai et al., 2005; Fang et al., 2009; Liu et al., 2011; He et al., 2015; and Daryabor et al., 2016).

The mean seasonal variability of surface hydrodynamics in the SCS was examined by taking temporal averages of the HYCOM-ROMS model results for the three-year period from 2012 to 2014 (**Figure S3**). The surface circulation field of the SCS is composed of basin-scale wind-generated circulations and gyres (**Figure S3c**, **d**), which are significantly affected by the seasonally varying Asian monsoons developed mainly near the Asian continent (**Figure S3a**, **b**). In winter, the mean surface currents showed a predominant cyclonic gyre in the northeastern part of the SCS (viz., east of the Gulf of Thailand) owing to the northeasterly energetic winter monsoon, with the strengthened southward-drifting western boundary current off the Vietnam coast (**Figure S3d**). In contrast, in summer, the northeastward currents directed towards the Taiwan Strait were derived from the northward-drifting western boundary current developed off the southern China coast, as a part of the broadly distributed northward SCS warm current provoked by the gentle southerly monsoon (**Figure S3c**, Zhu et al., 2019b). As the MP transport in the SCS is anticipated to vary substantially on the seasonal time scale, we subsequently investigated the seasonality in the MP transport in the SCS either by the near-surface currents exerted on buoyant (light) MPs or by the 3D currents responsible for the transport of the neutrally buoyant MPs that are fully passive to the ambient currents, followed by the analysis of the MP fractions transported out of the SCS.

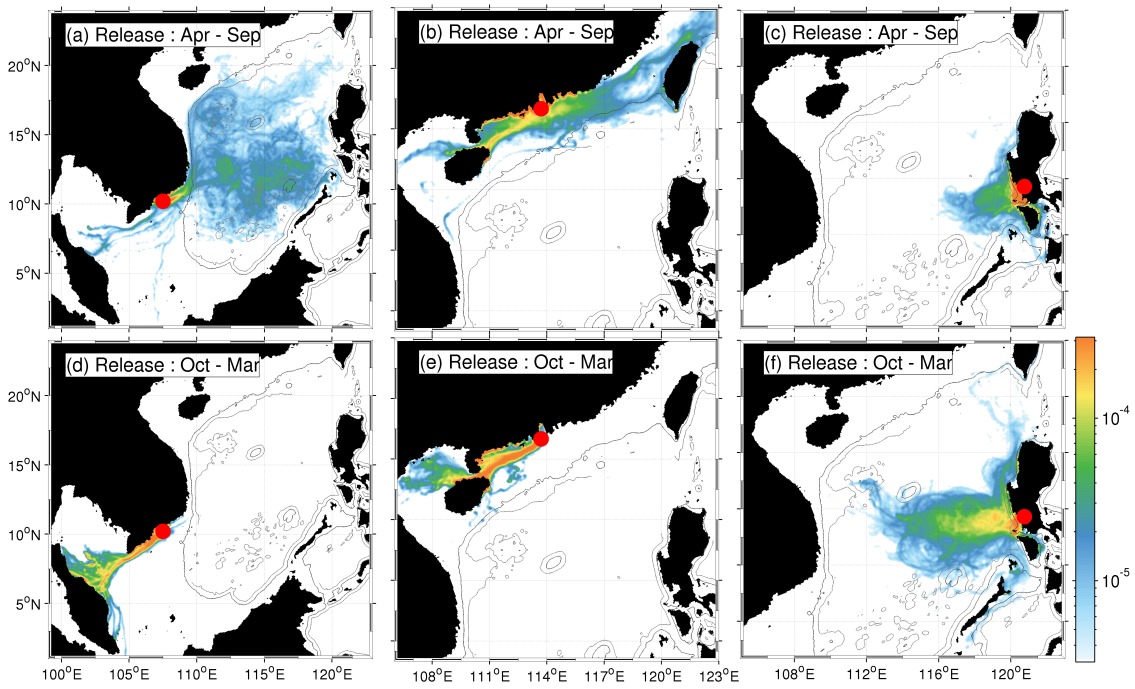

Figure 2. Lagrangian PDFs averaged over the advection time of 100 days (color). Top: For the MPs released from April to September. Bottom: For the MPs released from October to March. The sources of the MPs are mouths of (a) and (d): the Mekong River, (b) and (e): Pearl River, and (c) and (f): Pasig River, as depicted by red circle marks. Thin black contours are isobaths on 200 m and 1000 m.

3.2 Seasonality of the MP transport in the SCS

Figure 2 shows the two-dimensional horizontal distributions of the Lagrangian PDFs (see **Section S3**) of the buoyant MP particle displacement (i.e., Case 1) derived from the three rivers (i.e., the Pearl, Mekong, and Pasig rivers) in the SCS, averaged for the advection time of 100 days after each release. To account for the seasonal circulation variability examined in the preceding subsection, the time-averaged Lagrangian PDFs are grouped into two typical periods of particle emission: April to September, representing the summer condition when the gentle southwesterly monsoon is dominant, while October to March represents the winter condition when the intensive northeasterly monsoon prevails.

The buoyant MPs (Case 1) derived from the Mekong River in summer are transported northeastward by the coastal western boundary current and dispersed over a broad area in the SCS by distributed SCS warm currents when released during the prevailing southwesterly monsoon in summer (**Figure 2a**). On the other hand, the MPs released during the prevailing northeasterly monsoon in winter are transported southwestward and reach the coast of the Malay Peninsula and Gulf of Thailand with much less lateral dispersal (**Figure 2d**). This result is consistent with the field observations of Azman et al. (2021), in which higher concentrations of MP pollution along the coastline of the Malay Peninsula were measured during the northeasterly monsoon season.

The buoyant MPs derived from the Pearl River are dispersed in a strip over the continental shelf, showing prominent seasonality in dispersal patterns (**Figure 2b**, **e**). The cross-shelf transport in summer is less obvious than that from the Mekong River, as those from the Pearl River are more pronouncedly affected by the northeastward coastal currents (**Figure S3c**). During the summer monsoon, some MPs were transported further northeastward, passed through the Taiwan Strait, and eventually reached the ECS (**Figure 2b**). On the other hand, under the northeasterly monsoon in winter, most MPs were immediately transported southwestward, passed the northern coast of Hainan Island, and reached the Gulf of Tonkin (**Figure 2e**).

Such seasonal patterns in MP dispersal are well explained by wind-generated circulations induced by seasonally varying monsoons in this region. In the central part of the SCS, strong northeasterly winds blow from October to March, whereas relatively weaker southwesterly winds blow from April to September. The oceanic flow field in the SCS is predominantly composed of monsoon-induced wind-generated circulating gyres (Zhu *et al*. 2019b). In winter, the mean surface currents form a cyclonic gyre in the northern part of the SCS by the northeasterly coastal monsoon, which induces an elevated sea surface height near the shore, leading to a southward current off the Vietnam coast and a southeastward current off the southern China coast as a part of the intensified western boundary current. In turn, in summer, the western boundary current is reversed by the southerly to southwesterly monsoon to generate northeastward currents off the southern China coast as a part of the SCS Warm Current directed to the Taiwan Strait (Zhu *et al*. 2019b). The transport of MPs in the SCS is obviously affected by this seasonally varying circulation system.

There are distinctive seasonal differences in the transport distances of MPs released from the Pasig River. Compared to the summer condition (**Figure 2c**), the southwestward transport was enhanced, and the particles were broadly dispersed in the central part of the SCS during the northeasterly monsoon in winter (**Figure 2f**). Thus, in the SCS, MP transport is characterized by distinctive seasonality influenced by the prevailing monsoon over the sea. The MPs originating from the three major rivers are mostly transported over an extensive area in the SCS, while they also outflow to the surrounding seas to a certain extent for the three-year period from 2012 to 2014.

3.3 Effects of buoyancy and random-walk diffusivity on the MP transport

To investigate the buoyancy effects on the MP dispersal on a seasonal timescale, as well as the effects of under-resolved subgrid-scale eddy diffusivity on the 2DH Lagrangian transport commonly used in many previous modeling studies, we compared the horizonal Lagrangian PDFs for the three cases (Cases 1, 2, and 3) that were averaged for the advection time of 90 days after each MP release from the three major rivers (**Figure 3**). We note that the differences between Cases 1 and 2 are mainly caused by the random walk diffusivity considered only in Case 2, while those between Cases 1 and 3 are attributable to the vertical shear-induced dispersion effects in Case 3, in which vertically distributed MPs are advected differently by depth-dependent horizontal currents.

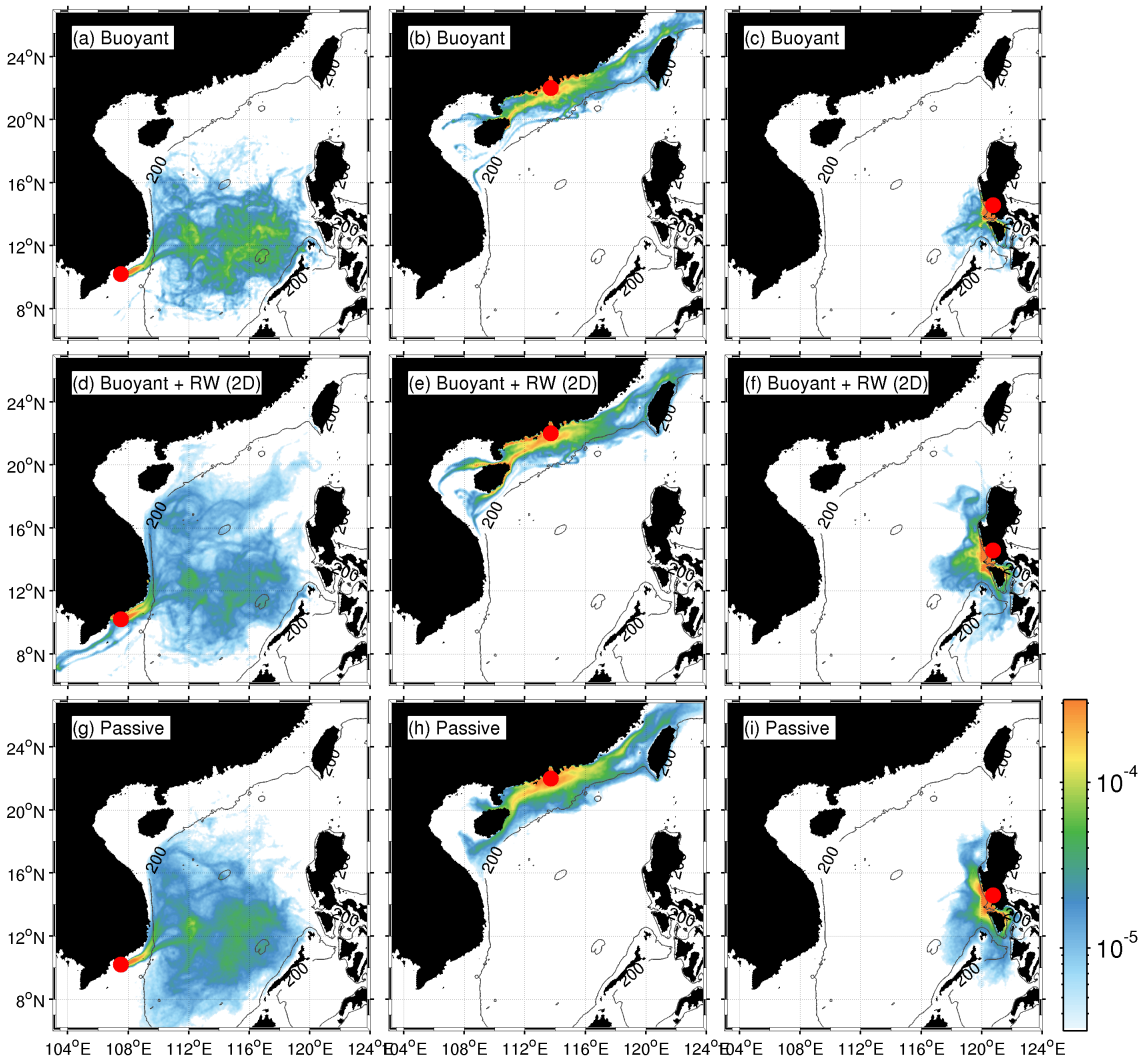

Figure 3. Lagrangian PDFs of the MPs released from April to September averaged over the advection time of 90 days (color). Top row: Case 1 (buoyant MPs), middle row: Case 2 (buoyant + random walk diffusivity) and bottom row: Case 3 (neutral and fully passive 3D MPs). Left column (a)-(c): MPs released from the Mekong River, middle column (d)-(f): from the Pearl River, and right column (g)-(i): from the Pasig River, where red circle marks are the release sites located at each of the three river mouths. Contours are isobaths on 200 m.

In general, regardless of the buoyancy and random walk effects, the MPs released from the three major rivers for all three cases are consistently transported primarily in the circulation direction in the SCS; the overall differences among the cases are rather minor. However, as expected, the horizontal extent of the non-buoyant MPs (Case 3; **Figure 3g–i**) is wider than that of the buoyant MPs (Case 1; **Figure 3a–c**) because of the influence of the depth-variant velocity magnitudes and directions in the spiraling surface Ekman boundary layer. In addition, the non-buoyant MPs are diluted more considerably in the vicinity of the source areas (i.e., the mouths of the three rivers) than the buoyant MPs. When the random walk lateral diffusivity is introduced (Case 2; **Figure 3d–f**), the horizontal extent of the MP dispersal is also slightly stretched farther, and the source area dilution occurs more apparently than those for Case 1, while the prevailing transport direction does not change significantly. Hence, we conclude that both the buoyant and neutrally buoyant MPs behave quite similarly in the horizontal

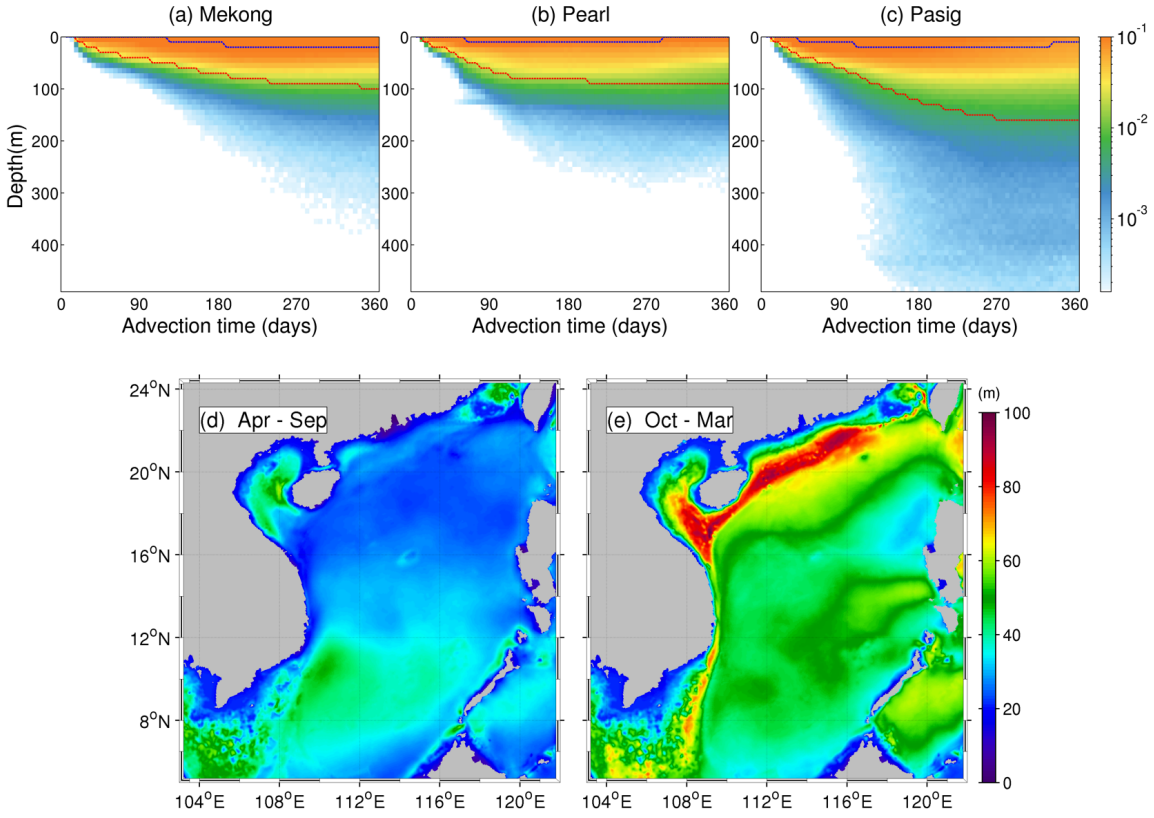

Figure 4. Top: Hovmöller diagrams of the vertical distribution of Lagrangian PDFs of the MPs integrated over the entire study area as a function of advection time until 360 days after the releases of the non-buoyant MPs (viz., Case 3) derived from (a) the Mekong River, (b) the Pearl River, and (c) the Pasig River from April to September. Blue and red dotted lines show the corresponding 50 and 95 percentiles. Bottom: Mixed layer depths for (d) April-September and (e) October to March, averaged for the three-year period of 2012-2014.

direction, yet with more effective lateral diffusivity inherent in the latter. The *ad hoc* random walk model appends further lateral diffusivity, although the overall dispersal patterns do not change substantially, implying that subgrid-scale mixing associated with submesoscale eddies may not be crucial for seasonal MP transport in the SCS.

Figure 4a–c shows temporal evolutions of the vertical distribution of the depth-dependent Lagrangian PDFs integrated spatially over the entire model domain of the neutrally buoyant MPs (Case 3) released from the three rivers that are transported passively to ambient currents, evaluated for every 10-m depth bin. Although the non-buoyant MPs are mostly suspended in the surface layer within a depth of 10 m from the surface, some particles are affected by both vertical mixing and advection and thus are distributed vertically as time progresses. The surface planetary boundary layer is often called the surface mixed layer, where vertical turbulent mixing is predominant. **Figure 4d–e** shows the mean mixed layer depths for the warm and cold seasons averaged over the three-year analysis period. The surface mixed layer develops more pronouncedly in the cold season to be deeper (approximately 50–100 m) owing to intensive convection by surface cooling as compared to that in the warm season (approximately 20–50 m). Even after one year (360 days) of advection time after the releases, approximately 50% of the particles are transported to depths of several tens of meters (roughly in the surface mixed layer), and

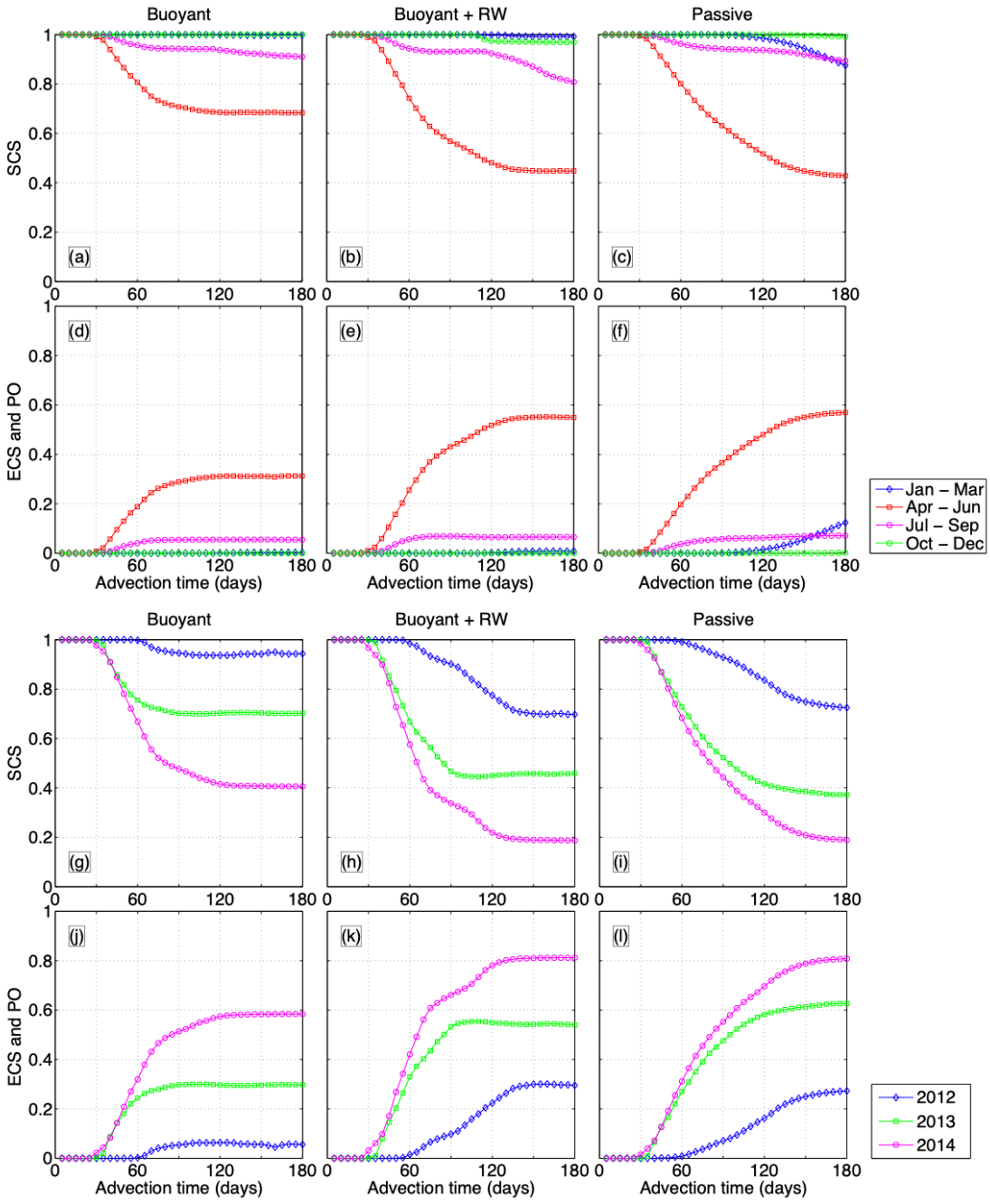

Figure 5. Fraction of MPs released from the Pearl River as a function of the advection time in day. Line colors correspond to the duration of the MP releases indicated in the legends. Top six panels: Seasonal variability for (a, d) Case 1 (buoyant MPs), (b, e) Case 2 (buoyant MPs + random walk diffusivity), and (c, f) Case 3 (passive MPs). (a, b, c) The fraction of MPs that remains in the SCS, and (c, d, e) that was transported to the East China Sea (ECS) and the Pacific Ocean (PO). Bottom six panels: Inter-annual variability for (g, j) Case 1, (h, k) Case 2, and (i, l) Case 3. The Pearl River-derived MPs released from April to June (g-i) that remain in the SCS and (j-l) that were transported to the ECS and the PO.

228 approximately 5% of MPs are transported to depths of 100 m to 400 m (below the mixed layer). In
229 particular, among the three sources, the MPs from the Pasig River dive the deepest; below the depth of
230 400 m (**Figure 4c**). These deep diving MPs may contribute to MP pollution in the middle and lower
231 layers of the SCS. Therefore, non-buoyant MPs that disappear from the surface layer but do not return

to the surface layer again (Kooi et al. 2017) are transported to the deep ocean, and may contribute to subsurface MP pollution observed down to depths of several hundred meters over a wide area of the SCS.

3.4 Destinations of the MPs derived from the Pearl River

In the Pearl River Estuary, China, the MP concentration was observed to be approximately 25 times higher than that in the central SCS (Cai et al., 2018; Lam et al., 2020). Thus, the MPs from the Pearl River are anticipated to have a significant influence on the distribution of MPs, especially in the northern SCS. Indeed, the model-predicted horizontal Lagrangian PDF distributions in **Figures 2b**, **2e**, **3b, 3e,** and **3h** show that the Pearl River-derived MPs were distributed mostly in the along-shelf directions over the continental shelf, whereas they were rarely transported seaward to the central SCS. In addition, when the MPs were released during the wet/warm season (from April to September) in southern China, many MPs were transported northeastward along the shore, passed through the Taiwan Strait, and reached the ECS (**Figure 2b**). This result clearly suggests that the Pearl River can be a source of MPs found in the ECS. Hence, we conducted further analysis of the fractions of the released MPs that reach the surrounding seas (the ECS, the Pacific Ocean, etc.) by passing several transects (mostly straits) that separate two seas, as shown by the red lines in the left panel of **Figure 1**, to quantify the MPs that remain in the SCS or those that are transported out of the SCS to the surrounding seas.

Figure 5a–f shows time series of the fractions of the Pearl River-derived MPs existing in the ECS and the Pacific Ocean (labeled as PO) for four quarterly releasing periods (January–March, April–June, July–September, and October–December) averaged over the three years of the model results for the buoyant MPs (Case 1), buoyant plus random walk (Case 2), and neutrally buoyant MPs (Case 3) until the advection time of 180 days after the releases. Evidently, the releases from April to June resulted in the largest MP discharge out of the SCS. During this period, the MPs, to be transported mostly to the ECS and the Pacific Ocean for half a year of the advection time, in the SCS decreased by approximately 30% (Case 1) or approximately 60% (Cases 2 and 3). In contrast, for the other three quarterly periods, the fractions of the MPs transported out of the SCS is very low and approximately 80–100% of the MPs released from the Pearl River remained in the SCS.

Subsequently, we focused on the inter-annual variability of the fraction of the Pearl River-derived MPs released from April to June for the three cases (**Figure 5g–l**). The difference among the cases is not as large as expected from the similarity in the lateral distributions of the Lagrangian PDFs shown in **Figure 3**, although the inter-annual variability is pronounced. The fractions of the MPs transported to the ECS and the Pacific Ocean for half a year of the advection time after the releases varied by approximately 5–60% (Case 1; buoyant), 30–80% (Case 2; buoyant plus random walk), and 25–80% (Case 3; neutrally buoyant and passive) of the total MPs released. During the wet/warm season (spring and summer) under the influence of relatively weak southerly winds but larger river discharges, the Pearl River plume is advected eastward and offshore by the coastal current induced by the upwelling-favorable winds (Dong et al., 2004: Bai et al., 2015). The MPs from the Pearl River transported through the Taiwan Strait to the ECS were increased owing to the Taiwan Strait Warm Current and the Taiwan

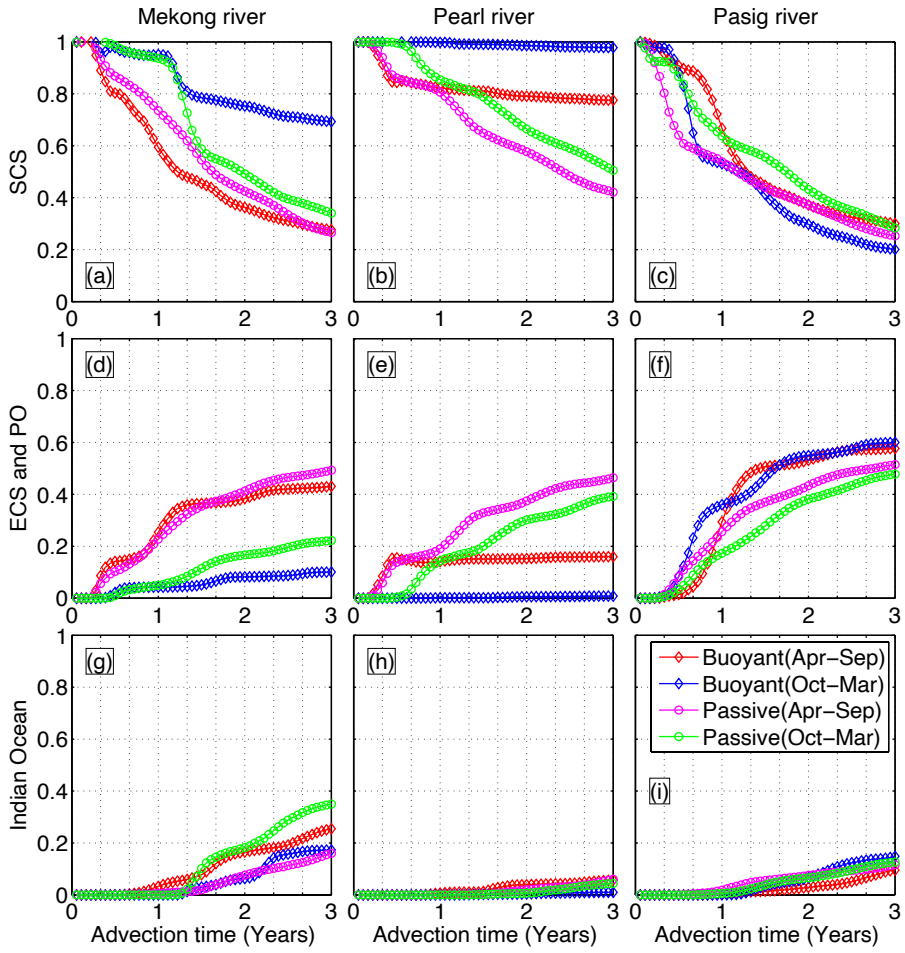

Figure 6. Fraction of MPs released from the (left) Mekong, (middle) Pearl, and (right) Pasig rivers as a function of the advection time in year. Line colors correspond to the imposed density of the MPs and the durations of the MP releases indicated in the legend in (i). Top: the fractions of MPs that remains in the SCS, middle: that were transported out to the East China Sea (ECS) and the Pacific Ocean (PO), and bottom: that were transported out to the Indian Ocean. Red and blue lines: Case 1 (buoyant MPs), magenta and green lines: Case 3 (passive MPs).

Warm Current, both of which are northeastward currents toward the ECS, and intensify in summer (Qi et al., 2017). Because approximately 80% of the annual discharge of the Pearl River occurs during the wet season (April–September; e.g., Yin et al., 2004), the MP emissions also increase then (Lebreton et al., 2017). Therefore, much of the MPs emitted during the southwesterly monsoon season in the SCS are anticipated to be transported from the SCS shelf to the ECS through the Taiwan Strait. In turn, the fraction of MPs remaining in the SCS increased by approximately 20% in Case 1 compared to Case 2 and Case 3. The cause of this increase is discussed in the next section.

4. Long-term MP transport

4.1. Long-term transported fractions of MPs

Isobe et al. (2019) numerically studied the surface MP concentrations across the Pacific Ocean for the next 50 years and showed that MP concentrations may increase in the seas around Japan and in

the central Northern Pacific over the next few decades. In their model, the MP transport was assumed to be driven purely by the surface currents; thus, vertical mixing and transport were omitted. However, after the advection time of approximately three years, these surface MPs were randomly eliminated to be consistent with the *in situ* surface MP concentrations. Apart from the practical importance of vertical MP transport, their study also suggested that oceanic MP transport could occur for a long period of time (approximately 3 years). Therefore, it is important to evaluate whether the MPs derived from the SCS would remain in the SCS or be transported to the open ocean and eventually to the surrounding seas for years. In Section 3, we see that the fraction of MPs derived from the Pearl River varies from year to year (**Figure 5**). Although the Pearl River-derived MPs tended to exit the SCS to the ECS in a couple of months, many of the MPs derived from the Mekong and Pasig rivers remained in the SCS (**Figures 2** and **3**).

Figure 6 shows the fractions of the MPs released from the three rivers remaining in the SCS (**Figure 6a**–**c**), reaching the ECS and Pacific Ocean (**Figure 6d**–**f**) and the Indian Ocean (**Figure 6g**–**i**) as a function of the elapsed advection time for the buoyant (Case 1) and passive (Case 3) MPs. The MP fractions were compiled into two groups depending on the time of release: the southwesterly monsoon (April to September) and the northeasterly monsoon (October to March) seasons, consistent with **Figure 2**. The MPs derived from the Mekong River released in the southwesterly monsoon season were dispersed broadly to the most extensive area in the SCS under the influence of the northeastward western boundary current developed in summer (**Figure 2a**), while they flowed from the SCS to the ECS and Pacific more rapidly than those released in the northeasterly monsoon season, regardless of the buoyancy of the MPs (**Figure 6a**, **d**). In contrast, less than 10% of the MPs are discharged to the ECS and the Pacific in the first year for the northeasterly monsoon season releases, demonstrating the coastal trap of the MPs near the Malay Peninsula (**Figure 2d**), followed by abrupt decreases in the remaining fraction in the second year with much stronger retention of the SCS for the buoyant MPs. The outflow rate is clearly determined by the semiannually reversing Asian monsoon. The MPs that remain in the SCS are retained over a wide area in the central part of the SCS by counterclockwise circulation in winter (Zhu et al., 2019. Also depicted in **Figure S3a**). Then, the outflowing fraction begins to increase again after approximately one year when the southwesterly monsoon starts to prevail (**Figure 6a**, **d**). Three years after the release in the southwesterly monsoon season, 40–50% of the MPs were discharged to the ECS and the Pacific (**Figure 6d**). The MPs released during the prevailing northeasterly monsoon from the Mekong River were transported predominantly southwestward (**Figure 2d**) with an outflow rate of only 10–20% to the ECS and Pacific (**Figure 6d**). Transport to the Indian Ocean was also observed in all periods and cases, ranging from 20–40% after three years of advection (**Figure 6g**).

The fraction of MPs derived from the Pearl River depends more significantly on the MP buoyancy than those derived from the other two rivers. The buoyant MPs that keep parking in the surface layer are obviously attributed to greater retention in the SCS (**Figure 6b**) and thus much less outflow to the ECS and the Pacific (**Figure 6e**) than the non-buoyant MPs. In fact, approximately 60% of the released non-buoyant MPs (Case 3) were discharged to the ECS and the Pacific after three years, regardless of the period of release, while approximately 20% (almost 0%) of the buoyant MPs were

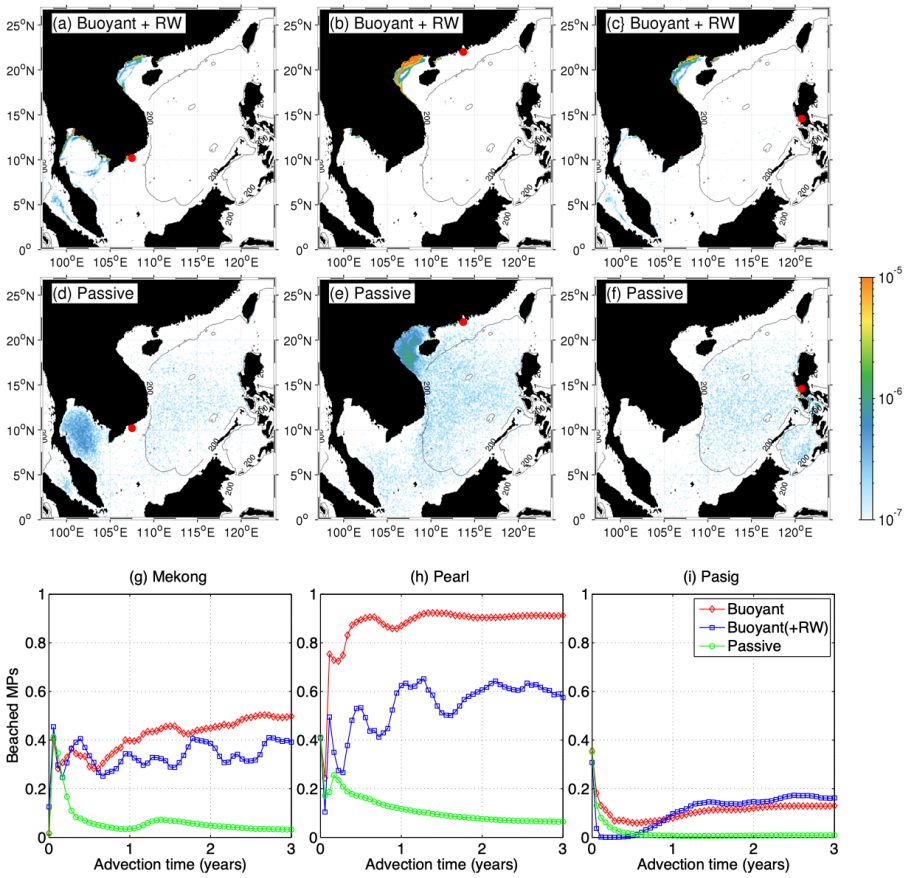

Figure 7. Long-term fate of the MPs. Top six panels (a-f): Lagrangian PDFs of the released MPs on the advection time of 3 years for (a-c) Case 2 (buoyant + random walk) and (d-f) Case 3 (fully passive MPs). Red circle marks correspond to the released sites, where (a) and (d) from the Mekong River, (b) and (e) from the Pearl River, and (c) and (f) from the Pasig River. Contours are isobaths on 200 m and 1000 m. Bottom three panels (g-i): The fraction of beached MPs derived from (g) the Mekong River, (h) the Pearl River, and (i) the Pasig River. The MP releases in 2012 are depicted here for the advection time of up to 3 years. Red, blue, and green lines are for Case 1, Case 2, and Case 3, respectively.

discharged to the ECS and the Pacific when they were released in the southwesterly (northeasterly) monsoon season.

The MPs derived from the Pasig River behaved most similarly for all the scenarios, among those derived from the three rivers (**Figure 6c**, **f**, **i**). The Pasig-derived MPs were extensively transported westward to the central part of the SCS for an advection time of a few months (**Figure 2c**) with more westward extent of the MP dispersal for the northeasterly monsoon season releases (**Figure 2f**). Nevertheless, the timing of the initial increase in the outflow rate to the ECS and Pacific differs from case to case (**Figure 6f**). For instance, the discharge rate of the buoyant MPs increases four–eight months for the northeasterly monsoon release (September to March), while from eight months to one year for the southwesterly monsoon release (April to September). At the advection time of three years, a large fraction of the released MPs outflow to the ECS and the Pacific, approximately 60% for the buoyant MPs, and 40–50% for the non-buoyant MPs. Thus, the MPs from the Pasig River were transported to the central SCS over tens to hundreds of days, and then to the ECS and the Pacific by the northeastward

current that occurred with the prevailing southwesterly monsoons. In addition, 10–15% of the MPs were transported to the Indian Ocean at the advection time of three years (**Figure 6i**).

4.2 Possible final destinations of the river-derived MPs

To examine the long-term fate of the river-derived MPs in the SCS, we examine the Lagrangian PDFs at the advection time of three years for the buoyant and non-buoyant MPs released from the three major rivers (**Figure 7**). The results for the non-buoyant, passive MPs (**Figure 7d**–**f**) are intuitively consistent with the results shown in **Figure 6**, which indicates that at least approximately 20% of the released MPs remained in the SCS. **Figure 7d**–**f** shows that the MPs remaining in the SCS mostly stay in the Gulf of Thailand (the Mekong-derived MPs), Gulf of Tonkin (the Pearl-derived MPs), and central SCS (the Pasig-derived MPs). In contrast, the buoyant MPs were visually missing in the SCS ocean, where the Lagrangian PDFs almost vanished (**Figure 7a**–**c**).

The mechanism behind this difference was simple. We found that the missing buoyant MPs were mostly beached. **Figure 7g**–**i** shows the time series of the fraction of beached MPs, in which they gradually vary except for the initial adjustment occurred in the first 2–3 months. Approximately 40–50% of the buoyant MPs derived from the Mekong River, approximately 60–90% of the Pearl River-derived MPs, and approximately 20% of the Pasig River-derived MPs have been beached. Beaching occurs rather promptly after the release of buoyant MPs, without prominent temporal evolutions. On the other hand, the non-buoyant MPs derived from the three rivers were barely beached at less than 10% of the released MPs. As a side remark, the random walk diffusivity places the nearshore MP particles away from the shore (i.e., forced to move offshore) that eventually diminishes the beached MPs.

These results indicate that the MPs released from the Pearl River, Mekong River, and Pasig River tend to be transported to the ECS and the northwest Pacific Ocean through the Luzon Strait and Taiwan Strait during the prevailing southwesterly monsoon. If the MPs remain in the SCS, many of them are transported to the shore and beached. In reality, the buoyant MPs that beached may repeatedly drift back and forth between the shore and the ocean, losing buoyancy under the influence of friction, fragmentation, and biofouling; eventually become non-buoyant MPs that are likely to be transported over a wide area again. However, such processes have not been modeled in the present study.

5. Discussion

5.1 Performance of the microplastic transport model

Although the HYCOM-ROMS model has been validated thoroughly as noted in **Section S1**, it is worthwhile to demonstrate the validity of the present simplified particle tracking model. Here we exploited a publicly available data set of satellite-tracked surface drifters distributed by the Global Drifter Program (GDP; Elipot et al., 2016), in which more than 30,000 drifters have been deployed and tracked in the global ocean from 2005 to the present at a quarter day interval. The accuracy of the particle tracking model is confirmed statistically by comparing the modeled Lagrangian PDFs with the trajectories of the GDP drifters that have existed in the SCS. **Figure 8** shows examples of such

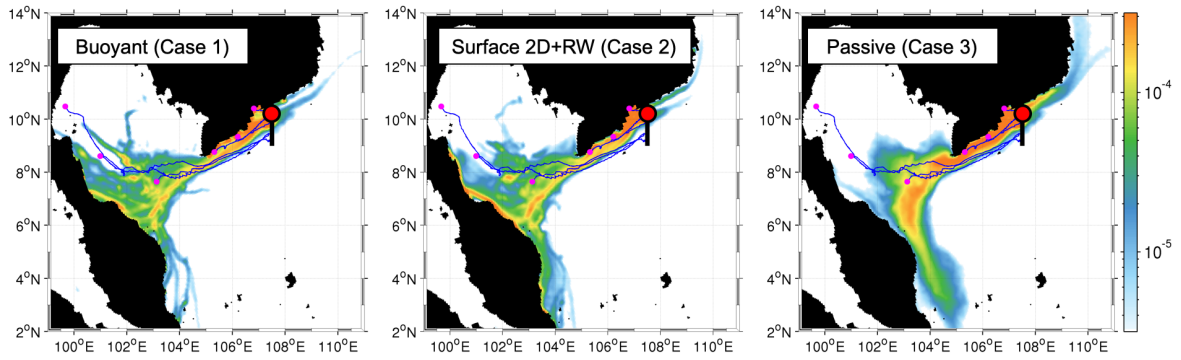

Figure 8. Same as **Figure 2d**, but six in situ surface drifters' trajectories (blue curves) and the final positions of them (magenta) are superposed on the Lagrangian PDFs averaged over the advection time of 120 days (color) for the MPs released from the Mekong River (red circle mark) from October to March. Left: Case 1 (buoyant MPs), middle: Case 2 (buoyant + random walk diffusivity), and right: Case 3 (neutral and fully passive 3D MPs).

comparisons for the particles released from Mekong River. We set a transect (107.5°E and 9°N - 10.5°N) near the mouth to search for the GDP drifters that passed through the transect from 2012 to 2014. Six drifters were detected, while all of them occurred in colder seasons (October to March), not in warmer seasons. To be consistent with the extracted drifter data, the time-averaged Lagrangian PDFs are computed for the modeled particles released from October to March. Three model results are represented in **Figure 8**, whereas Cases 1 and 2 correspond to the drifters that stay at the ocean surface. Three drifters out of six traveled shorter distances than the others and beached on the southern coast near the tip of the Indochina Peninsula, where the Lagrangian PDFs are very high. The other three drifters were further transported westward to enter the inner Gulf of Thailand and approximately followed the areas with higher Lagrangian PDFs. These results evidently indicate that the present particle tracking model performed quite well with good accuracy for Cases 1 and 2. In contrast, modest discrepancy is found for Case 3 because it represents fully passive MPs and thus is unsuitable to compare with surface drifters. Interestingly, the passive MPs in Case 3 were transported more to the south off the Malay Peninsula than those for the near-surface MPs in Cases 1 and 2. This result demonstrates again that the buoyancy of the MPs affects their lateral transport patterns substantially.

5.2 Fate of the river-derived microplastics

In the SCS, pronounced seasonality was observed in the medium-term (i.e., seasonal timescale) transport of MPs and the outflowing fractions to the surrounding seas. Therefore, MP pollution in these areas may vary greatly depending on the season. Field observations with respect to MPs have normally been conducted for a few months in the SCS (Cai et al., 2017) and the seas around Japan (Isobe et al., 2015), whereas year-round monitoring is required to clarify the seasonal distribution of MPs.

The large meso plastic (>5 mm) suspended in the Japan Sea was reported to be influenced by the prevailing southeastward Stokes drift in the surface layer and was pushed to the coast of the Japanese islands (Iwasaki et al., 2017). On the other hand, smaller MPs (<5 mm) were transported broadly over

an extensive area of the Japan Sea by the northeastward current, because they were not affected by the Stokes drift velocity, which is generally intensified in the surface layer, but rather their vertical distribution was extended to a depth of several meters by vertical mixing (Iwasaki et al., 2017). The present study indicated that buoyant MPs from the Pearl River were beached more considerably than the non-buoyant MPs. The buoyant MPs are expected to drift in the surface layer of the ocean, to repeatedly exchange with the shore, to increase their own density through biofouling and degradation by ultraviolet rays and friction (Kaiser et al., 2017: Fazey et al., 2016), and eventually lose their buoyancy, thereby increasing their horizontal dispersal distance (Isobe et al., 2014).

In addition, a greater fraction of the non-buoyant MPs was transported to the ECS and Pacific Ocean when the MPs were advected for long periods of time. If we assume a large meso-plastic, the percentage of shoreward MP transport may even be higher owing to the influence of Stokes drift in the surface layer. However, because the wave-driven littoral currents in and around the surf zone where waves break are much more complicated and completely different from the non-wave current field (Uchiyama et al., 2010; 2017a), a simple linear addition of the Stokes drift velocity to the non-wave Eulerian velocity could cause large errors in the transport estimation, particularly with numerical models. This discrepancy is similarly anticipated in offshore MP transport where the Stokes-Ekman currents develop, as pointed out in **Section S2**. On a global scale, Stokes drift may not contribute to the large-scale accumulation of microplastics in the subtropics rather than Ekman currents and geostrophic currents because of its non-divergent nature. In turn, Stokes drift may lead to increased transport to polar regions where storm-generated waves are larger and occur more frequently (Onink et al., 2019). We showed that the MPs suspended in the SCS were transported in the same direction as the monsoon as the western boundary currents of the basin-scale wind-generated gyre. Because Stokes drift associated with wind waves mainly occurs in the same direction as the sea wind (van Sebille et al., 2020), an *ad hoc* linear addition of Stokes drift to the HYCOM-ROMS model-generated Eulerian velocity results in enhancement of downwind extent of the MP transport in the SCS, or leads to very minor effects as seen in **Section S4**. Therefore, the effects of waves on MP transport are still underway and must be carefully studied in the future.

Once MPs are transported shoreward from the offshore, some are beached permanently, and some are possibly reverted back to the offshore by back-rushing waves and offshore headed currents such as rip currents after a certain period of time (Hinata et al., 2017). The residence time at the shore estimated by observations (Hinata et al., 2017) led to the development of a model for the behavior of MPs near the shore (Hinata et al., 2020). Hence, more realistic beaching modeling is necessary in the future to accurately reproduce the nearshore processes and retention for MP transport along with a wave-averaged 3D circulation model requisite, particularly for surf zone applications.

In previous modeling studies on MP transport, beaching was sometimes considered (Zhang et al., 2020), but was omitted at other times (Isobe et al., 2019; van Sebille et al., 2019; Onink et al., 2019). This study employs a simple beaching model that represents the resolved “stickiness” of the shore by bilinear interpolation of lateral currents that decrease towards the shore where velocity vanishes, while neglecting the complicated nearshore physics responsible for actual beaching processes. The random

walk model used in Case 2 serves as a stochastic redistributor of the nearshore MPs to drift back offshore, which leads to diminishing the beached MPs by approximately 20–50% relative to Case 1 (**Figure 7g**–**i**). On the other hand, the decrease in the beached MP fraction is apparent in Case 3, demonstrating that buoyant MPs (Cases 1 and 2) beaches much more frequently than non-buoyant MPs (Case 3). Because of the difference in the weight density of the MPs, the buoyant MPs are confined in the surface layer, while the non-buoyant MPs can spread over a wider depth range (**Figure 4a**–**c**). In the surface layer, the intensive southwestward wind blowing in the southern China coastal areas promotes the onshore Ekman flow to be approximately perpendicular to the continent. Thus, the buoyant MPs in the surface layer derived from the Pearl River are transported to the coastal area owing to wind-induced currents that are largely influenced by the northerly to northeasterly monsoon (**Figure S3**), attributed to more beached MPs (**Figure 7h**). In contrast, the direction of the subsurface currents at a depth of 5 m is rather in the along-shelf direction with a much weaker velocity (not shown). Hence, the non-buoyant MPs distributed widely in the vertical direction (**Figure 4a**–**c**) are affected by subsurface currents, which do not promote onshore transport and thus less beaching occurs. This result suggests that the buoyancy of the MP particles alters their mean vertical positions, resulting in being driven by different horizontal current velocities and directions in the spiraled Ekman boundary layer.

The seafloor is considered to be a reservoir of MPs because MPs that lose their buoyancy will reach the seafloor (Woodall et al., 2014). A field survey conducted on the continental shelf in the coastal area of southern China confirmed that MP contamination occurs on the seabed over an extensive area on the shelf (Chen et al., 2020). Our model results for the neutrally buoyant MPs (Case 3) showed that the MPs gradually migrate vertically down below the surface mixing layer developed approximately 20–50 m (spring/summer) and approximately 50–100 m (fall/winter) from the surface (**Figure 4d, e**). Consequently, more than 5% of the released MPs were transported deeper than 100 m (**Figure 4a**–**c**). If the weight density of MPs increases to be negatively buoyant, that is, to have a downward settling velocity, more MPs are able to dive below the mixed layer to possibly reach the abyssal ocean. For instance, Fazey and Ryan (2016) estimated that after 17 to 66 days, approximately half of the MPs suspended in coastal areas start to have a settling velocity, while Kaiser et al. (2017) estimated that this happens after approximately six weeks.

We examined MP contamination on the seafloor in the SCS based on the results of the non-buoyant MP model. The MPs derived from the Pearl River were broadly transported over the continental shelf (**Figure 4h**), and thus have a large chance to contribute to MP pollution on the continental shelf seabed, consistent with the observations of Chen et al. (2020). On the other hand, the MPs derived from the Mekong and Pasig rivers were mostly transported to the central SCS in the advection time of several tens of days (**Figure 3g**, **i**). If these MPs started to have a settling velocity, they could dive into the deep abyssal oceans at depths of several thousand meters. However, there are many unanswered questions about the processes by which MPs acquire settling velocity in the ocean, and further research is needed to understand MP pollution in the deep oceans.

6. Conclusions

In the SCS, it was confirmed that the transport pattern of MPs is substantially influenced by the seasonally varying, basin-scale wind-driven circulation system induced by the prevailing monsoon system developed on the Asian continent. The mean transport direction of the river-derived MPs, particularly those from the Pearl and Mekong rivers, was found to be northeastward (southwestward) during the periods of prevailing southwesterly (northeasterly) monsoon. MPs released from the southern coast of China manifest a large proportion of discharge into the East China Sea (ECS) across the Taiwan Strait, suggesting that they might be one of MP sources observed in the seas around Japan.

We found that the rate of lateral MP transport has non-trivial interannual variability, presumably owing to the long-term variability of the Asian monsoon and the associated weather system that alter the SCS circulations as main driving forces. As the advection time progressed from several months to several years, few MPs remained in the SCS, whereas a large fraction of the MPs from the Mekong and Pasig rivers were transported to the ECS and Pacific Ocean, of which some slightly leaked into the Indian Ocean. The long-term northward transport to the ECS and the Pacific is evident, particularly during the southwesterly monsoon, indicating that the summer monsoon plays a significant role in the dispersal and advective distribution of MPs in the extensive area. Therefore, the SCS, which has many important emission sources of plastic waste to the ocean, is anticipated be a major source of MPs in the world's oceans.

Although approximately half of the non-buoyant MPs were found within a depth of 10 m from the surface, the remaining MPs were transported down to 10–100 m from the surface. More than 5% of the non-buoyant MPs sank down below a depth of 100 m, and some reached 400 m depth, suggesting that the MPs attaining negative buoyancy with a downward settling velocity may be a contributor to abyssal MP contamination. The buoyant MPs drifting on the continental shelf originating from southern China tend to be pushed toward the shore by northward wind-induced currents more pronouncedly than the non-buoyant MPs, which, in contrast, diffuse to deeper layers owing to vertical mixing and vertical advection. This result suggests that differences in the weight density of MPs affect their beaching processes and thus plastic pollution on beaches.

Acknowledgments

This research was financially supported by the Japan Society for the Promotion of Science (JSPS) Grant-in-Aid for Scientific Research (Grant # 18H03798) at Kobe University.

References

Azman, M.A., Ramli, M.Z., Othman, S.F.C., Shafiee, S.A., 2021. The distribution of marine debris along the Pahang coastline, Malaysia during the Southwest and Northeast Monsoons. Mar. Pollut. Bull. 170, 112630. https://doi.org/10.1016/j.marpolbul.2021.112630

Bai, Y., Huang, T.H., He., X., Wang., S.L., Hsin, Y.C., Wu, C.R., Zhai, W., Lui, H.K., Chen, C.T.A., 2015. Intrusion of the Pearl River plume into the main channel of the Taiwan Strait in summer. Journal of Sea Research. 95, 1–15. https://doi.org/10.1016/j.seares.2014.10.003

Buijsman, M., Uchiyama, Y., McWilliams, J.C. and Hill-Lindsay, C.R., 2012. Modeling semiduirnal internal tides in the Sourthern California Bight, J. Phys. Oceanogr., Vol.42, 62–77. http://dx.doi.org/10.1175/2011JPO4597.1

Cai, M., He, H., Liu, M., Li, S., Tang, G., Wang, W., Huang, P., Wei, G., Lin, Y., Chen, B., Hu, J., Cen, Z., 2018. Lost but can't be neglected: huge quantities of small microplastics hide in the South China Sea. Sci. Total Environ. 633, 1206–1216. https://doi.org/10.1016/j.scitotenv.2018.03.197

Cai, S., Liu, H., Li, W. and Long, X., 2005. Application of LICOM to the numerical study of water exchange between the South China Sea and its adjacent oceans. Acta Oceanol. Sin., **24**, 10–19.

Carr, S. D., Capet, X., McWillimas, J. C., Pennington, J. T., Chazez, F. P., 2008. The influence of diel vertical migration on zooplankton transport and recruitment in an upwelling region: Estimates from a coupled behavioral-physical model. Fish. Oceanogr. 17:1, 1–15. https://doi.org/10.1111/j.1365-2419.2007.00447.x

Chen, M., Du, M., Jin, A., Chen, S., Dasgupta, S., Li, J, Xu, H., Ta, K., Peng, K., 2020. Forty-year pollution history of microplastics in the largest marginal sea of the western Pacific. Geochem. Persp. Let, 13, 42-47.

Chu, P. C., Edmons, N. L. and Fan, C., 1999. Dynamical Mechanisms for the South China Sea Seasonal Circulation and Thermohaline Variabilities, J. Phys. Oceanogr., **29:11**, 2971-2989, https://doi.org/10.1175/1520-0485(1999)029<2971:DMFTSC>2.0.CO;2

Chubarenko, I., Bagaev, A., Zobkov, M., Esiukova, E. 2016. On some physical and dynamical properties of microplastic particles in marine environment. Mar. Pollut. Bull. 108, 105–112. https://doi.org/10.1016/j.marpolbul.2016.04.048

Daryabor, F., Ooi, S.H., Samah, A.A. and Akbari, A., 2016. Dynamics of the Water Circulations in the Southern South China Sea and Its Seasonal Transports. PLoS ONE, **11(7)**, e0158415, https://doi.org/10.1371/journal.pone.0158415

Dauhajre, D.P., McWilliams, J.C. and Uchiyama, Y., 2017. Submesoscale coherent structures on the continental shelf, J. Phys. Oceanogr., Vol. 47, pp. 2,949 - 2,976. http://dx.doi.org/10.1175/JPO-D-16-0270.1

Dong, L., Su, J., Wong, L.A., Cao, Z., Chen, J.C., 2004. Seasonal variation and dynamics of the Pearl River plume. Continental Shelf Research. 24, 1761-1777. https://doi.org/10.1016/j.csr.2004.06.006

Elipot, S., Lumpkin, R., Perez, R. C., Lilly, J. M., Early, J. J., Sykulski, A. M., 2016. A global surface drifter data set at hourly resolution, J. Geophys. Res. Oceans, 121, 2937–2966, https://doi.org/10.1002/2016JC011716

Emmerik, T., Klaveren, J., Meijer, L.J.J., Krooshof, J, W., Palmos, D.A.A., Tanchuling, M.A., 2020. Manila River Mouths Act as Temporary Sinks for Macroplastic Pollution. Front. Mar. Sci. 7, 545812. https://doi.org/10.3389/fmars.2020.545812

Fang, G., Wang, Y., Wei, Z., Fang, Y., Qiao, F. and Hu, X., 2009. Interocean circulation, heat and freshwater budgets of the South China Sea based on a numerical model. Dynam. Atmos. Oceans., **47**, 55–72. https://doi.org/10.1016/j.dynatmoce.2008.09.003

Fang, G., Susanto, R.D., Wirasantosa, S., Qiao, F., Supangat, A., Fan, B. Wei, Z. Sulistiyo, B. and Li, S., 2010. Volume, heat and freshwater transports from the South China Sea to Indonesian seas in the boreal winter of 2007–2008. J. Geophys. Res., **115**, C12. https://doi.org/10.1029/2010JC006225

Fazey, F.M.C., Ryan, P.G., 2016. Biofouling on buoyant marine plastics: An experimental study into the effect of size on surface longevity. Environmental Pollution. 210, 354–360. http://dx.doi.org/10.1016/j.envpol.2016.01.026

He, Z., Feng, M., Wang, D. and Slawinski, D., 2015. Contribution of the Karimata Strait transport to the Indonesian Throughflow as seen from a data assimilation model. Cont. Shelf Res., **92**, 16–22. http://dx.doi.org/10.1016/j.csr.2014.10.007

Hinata, H., Mori, K., Ohno, K., Miyao, Y., Kataoka, T., 2017. An estimation of the average residence times and onshore-offshore diffusivities of beached microplastics based on the population decay of tagged meso- and macrolitter. Mar. Pollut. Bull. 122, 17–26. https://doi.org/10.1016/j.marpolbul.2017.05.012

Hinata, H., Sagawa, N., Kataoka, T., Takeoka, H., 2020. Numerical modeling of the beach process of marine plastics: A probabilistic and diagnostic approach with a particle tracking method. Mar. Pollut. Bull. 122, 17–26. https://doi.org/10.1016/j.marpolbul.2020.110910

Hu, J., Kawamura, H., Hong, H. and Qi, Y., 2000. A Review on the Currents in the South China Sea: Seasonal Circulation, South China Sea Warm Current and Kuroshio Intrusion, J. Oceanogr., **56**, 607-624. https://doi.org/10.1023/A:1011117531252

Isobe, A., Kubo, K., Tamura, Y., Kako, S., Nakashima, E., Fujii, N., 2014. Selective transport of microplastics and mesoplastics by drifting in coastal waters. Mar. Pollut. Bull. 89, 324–330. http://dx.doi.org/10.1016/j.marpolbul.2014.09.041

569 Isobe, A., Uchida, K., Tokai, T., Iwasaki, S., 2015. East Asian seas, a hot spot of pelagic microplastics.
570 Mar. Pollut. Bull. 101, 618–623. https://doi.org/10.1016/j.marpolbul.2015.10.042

571 Isobe, A., Iwasaki, S., Uchida, K., Tokai, T., 2019. Abundance of non-conservative microplastics in the
572 upper ocean from 1957 to 2066. Nat. Commun. 10, 417. https://doi.org/10.1038/s41467-019-
573 08316-9

574 Iwasaki, S., Isobe, A., Kako, S., Uchida, K., Tokai, T., 2017. Fate of microplastics and mesoplastics
575 carried by surface currents and wind waves: a numerical model approach in the sea of Japan. Mar.
576 Pollut. Bull. 121, 85–96. http://dx.doi.org/10.1016/j.marpolbul.2017.05.057

577 Jambeck, J.R., Geyer, R., Wilcox, C., Siegler, T.R., Perryman, M., Andrady, A., Narayan, R., Law, K.L.,
578 2015. Plastic waste inputs from land into the ocean. Science. 347, 768–771.
579 http://dx.doi.org/10.1126/science.1260352

580 Kaiser, D., Kowalski, N., Waniek, J. J., 2017. Effects of biofouling on the sinking behavior of
581 microplastics. Environ. Res. Lett. 12, 124003. https://doi.org/10.1088/1748-9326/aa8e8b

582 Kamidaira, Y., Uchiyama, Y. and Mitarai, S., 2017. Eddy-induced transport of the Kuroshio warm water
583 around the Ryukyu Islands in the East China Sea, Cont. Shelf Res., 143, 206–218,
584 https://doi.org/10.1016/j.csr.2016.07.004

585 Kamidaira, Y., Uchiyama, Y., Kawamura, H., Kobayashi, T., Furuno, A., 2018. Submesoscale mixing
586 on initial dilution of the radionuclides released from the Fukushima Dai-ichi nuclear power plant.
587 Journal of Geophysical Research: Oceans. 123, 2808–2828.
588 https://doi.org/10.1002/2017JC013359

589 Kamidaira, Y., Kawamura, H., Kobayashi, T. and Uchiyama, Y., 2019. Development of regional
590 downscaling capability in STEAMER ocean prediction system based on multi-nested ROMS
591 model, J. Nuclear Sci. Tech., 56 (8), 752-763. https://doi.org/10.1080/00223131.2019.1613269

592 Kamidaira, Y., Uchiyama, Y., Kawamura, H., Kobayashi, T. and Otosaka, S., 2021. A modeling study
593 on the oceanic dispersion and sedimentation of radionuclides off the coast of Fukushima, J.
594 Environ. Radioact., 106724, 238–239. https://doi.org/10.1016/j.jenvrad.2021.106724

595 Kooi, M., van Nes, E.H., Scheffer, M., Koelmans, A.A., 2017. Ups and downs in the ocean: effects of
596 biofouling on the vertical transport of microplastics. Environ. Sci. Technol. 51, 7963–7971.
597 https://doi.org/10.1021/acs.est.6b04702

598 Kukulka, T., Proskurowski, G., Morét-Ferguson, S., Meyer, D.W., Law, K.L., 2012. The effect of wind
599 mixing on the vertical distribution of buoyant plastic debris. Geophys. Res. Lett. 39, 7601.
600 https://doi.org/10.1029/2012GL051116

601 Kurosawa, K., Uchiyama, Y., and Kosako, T., 2020. Development of a numerical marine weather routing
602 system for coastal and marginal seas using regional oceanic and atmospheric simulations, Ocean
603 Eng., 195, 106706. https://doi.org/10.1016/j.oceaneng.2019.106706

Lam, T.W.L., Fok, L., Lin, L., Xie, Q., Li, H-X., Xu, X-R., Ling, C-Y., 2020. Spatial variation of floatable plastic debris and microplastics in the Pearl River Estuary, South China. Mar. Pollut. Bull. 158, 111383. https://doi.org/10.1016/j.marpolbul.2020.111383

Lebreton, L. C., Van Der Zwet, J., Damsteeg, J. W., Slat, B., Andrady, A., Reisser, J., 2017. River plastic emissions to the world's oceans. Nat. Commun. 8, 1–10. https://doi.org/10.1038/ncomms15611

Li, D., Liu, K., Li, C., Peng, G., Andrady, A., Wu, T., Zhang, Z., Wang, X., Song, Z., Zong, C., Zhang, F., Wei, N., Bai, M., Zhu, L., Xu, J., Wu, H., Wang, L., Chang, S., Zhu, W., 2020. Profiling the Vertical Transport of Microplastics in the West Pacific Ocean and the East Indian Ocean with a Novel in Situ Filtration Technique. Environ. Sci. Technol. 54, 12979-12988. https://doi.org/10.1021/acs.est.0c02374

Liu, Q., Feng, M., and Wang, D., 2011. ENSO-induced interannual variability in the southeastern South China Sea. J. Oceanogr. **67**, 127–133. https://doi.org/10.1007/s10872-011-0002-y

Mason, E., Molemaker, J., Shchepetkin, A. F., Colas, F., McWilliams, J. C., Sangrà, P., 2010. Procedures for offline grid nesting in regional ocean models. Ocean Modelling. 35(1), 1–15.

Masunaga, E., Uchiyama, Y., Suzue, Y. and Yamazaki, H., 2018. Dynamics of internal tides over a shallow ridge investigated with a high-resolution downscaling regional ocean model, Geophys. Res. Lett., Vol. 45, No. 8, pp. 3550-3558, http://dx.doi.org/10.1002/2017GL076916

Masunaga, E., Uchiyama, Y. and Yamazaki, H., 2019. Strong internal tides generated by the interaction of the Kuroshio Current and tides over a shallow ridge, J. Phys. Oceanogr., 49 (11), 2917–2934. https://doi.org/10.1175/JPO-D-18-0238.1

Mato, Y., Isobe, T., Takada, H., Kanehiro, H., Ohtake, C., Kamimura, T., 2001. Plastic resin pellets as a transport medium for toxic chemicals in the marine environment. Environ. Sci. Technol. 35, 318–324. https://doi.org/10.1021/es0010498

Meijer, L.J.J., van Emmerik, T., van der Ent, R., Schmidt, C. and Lebreton, L., 2021. More than 1000 rivers account for 80% of global riverine plastic emissions into the ocean, Sci. Adv., **7:18**, https://doi.org/10.1126/sciadv.aaz5803

Mitarai, S., Siegel, D. A., Watson, J. R., Dong, C., McWilliams, J. C., 2009. Quantifying connectivity in the coastal ocean with application to the Southern California Bight. Journal of Geophysical Research. 114, C10026. https://doi.org/10.1029/2008JC005166

Onink, V., Wichmann, D., Delandmeter, P., van Sebille, E., 2019. The role of Ekman currents, geostrophy and Stokes drift in the accu- mulation of floating microplastic, J. Geophys. Res.-Oceans, 124, 1474–1490, https://doi.org/10.1029/2018JC014547

Piccardo. M., Renzi, M., Terlizzi, A., 2020. Nanoplastics in the oceans: Theory, experimental evidence and real world. Mar. Pollut. Bull. 157, 111317. https://doi.org/10.1016/j.marpolbul.2020.111317

Poulain, M., Mercier, M.J., Brach, L., Martignac, M., Routaboul, C., Perez, E., Desjean, M. C., ter Halle,

A., 2019. Small microplastics as a main contributor to plastic mass balance in the north atlantic subtropical gyre. Environ. Sci. Technol. 53, 1157–1164. https://doi.org/10.1021/acs.est.8b05458

Qi, J., Yin, B., Zhang, Q., Yang, D., Xu, Z., 2017. Seasonal variation of the Taiwan Warm Current Water and its underlying mechanism. Chin. J. Ocean. Limnol. 35, 1045–1060. http://dx.doi.org/10.1007/s00343-017-6018-4

Reisser, J., Slat, B., Noble, K., du Plessis, K., Epp, M., Proietti, M., de Sonneville, J.,Becker, T., Pattiaratchi, C., 2015. The vertical distribution of buoyant plastics at sea: an observational study in the North Atlantic Gyre. Biogeosciences. 12, 1249-1256. https://doi.org/10.5194/bg-12-1249-2015

Romero, L., Uchiyama, Y., Ohlmann, C., McWilliams, J. C., Siegel, D. A., 2013. Particle-pair dispersion in the Southern California coastal zone. Journal of Physical Oceanography, 43, 1862–1879. https://doi.org/10.1175/JPO-D-13-011.1

Shchepetkin, A.F., McWilliams, J.C., 2005. The regional ocean modeling system (ROMS): a split-explicit, free-surface, topography-following-coordinate oceanic model. Ocean Model. 9, 347–404. https://doi.org/10.1016/j.ocemod.2004.08.002

Shchepetkin, A.F., McWilliams, J.C., 2009. Computational kernel algorithms for fine- scale, multiprocess, longtime oceanic simulations. In: Temam, R., Tribbia, J. (Eds.), Handbook of Numerical analysis Vol. 14: Computational Methods for the Ocean and the Atmosphere. Elsevier, Amsterdam, pp. 119–181. https://doi.org/10.1016/S1570-8659(08)01202-0

Song, Y.T., 2006. Estimation of interbasin transport using ocean bottom pressure: theory and model for Asian marginal seas. J. Geophys. Res., **111**, C11, https://doi.org/10.1029/2005JC003189

Sun, X., Li, Q., Zhu, M., Liang, J., Zheng S., Zhao, Y., 2017. Ingestion of microplastics by natural zooplankton groups in the northern South China Sea. Mar. Pollut. Bull. 115, 217-224. https://doi.org/10.1016/j.marpolbul.2016.12.004

Tada, H., Uchiyama, Y., Masunaga, E., 2018. Impacts of two super typhoons on the Kuroshio and marginal seas on the Pacific coast of Japan. Deep-Sea Research Part I. 132, 80–93. https://doi.org/10.1016/j.dsr.2017.12.007

Takeda, N., Kashima, M., Odani, S., Uchiyama, Y., Kamidaira, Y. and Mitarai, S., 2021. Identification of coral spawn source areas around Sekisei Lagoon for recovery and poleward habitat migration by using a particle‐tracking model, Sci. Rep., 11, 6963. https://doi.org/10.1038/s41598-021-86167-5

Uchiyama, Y., McWilliams, J.C. and Shchepetkin, A.F. 2010. Wave-current interaction in an oceanic circulation model with a vortex force formalism: Application to the surf zone, Ocean Modelling, 34:1-2, 16-35. https://doi.org/10.1016/j.ocemod.2010.04.002

Uchiyama, Y., Idica, E., McWilliams, J. C., Stolzenbach, K. D., 2014. Wastewater effluent dispersal in

674 Southern California bays. Continental Shelf Research. 76, 36–52.
675 https://doi.org/10.1016/j.csr.2014.01.002

676 Uchiyama, Y., McWilliams, J. C., Akan, C. 2017a. Three-dimensional transient rip currents:
677 Bathymetric excitation of low-frequency intrinsic variability. Journal of Geophysical Research:
678 Oceans. 122, 5826–5849. https://doi.org/10.1002/2017JC013005

679 Uchiyama, Y., Suzue, Y., Yamazaki, H., 2017b. Eddy-driven nutrient transport and associated upper-
680 ocean primary production along the Kuroshio. Journal of Geophysical Research: Oceans. 122,
681 5046–5062. https://doi.org/10.1002/2017JC012847

682 Uchiyama, Y., Kanki, R., Takano, A., Yamazaki, H., Miyazawa, Y., 2018a. Mesoscale reproducibility in
683 regional ocean modeling with a 3-D stratification estimate based on Aviso-Argo data.
684 Atmosphere-Ocean. 56(4), 212–229. https://doi.org/10.1080/07055900.2017.1399858

685 Uchiyama, Y., Odani, S., Kashima, M., Kamidaira, Y., Mitarai, S., 2018b. Influences of the Kuroshio on
686 interisland remote connectivity of corals across the Nansei Archipelago in the East China Sea. J.
687 Geophys. Res. Oceans. 123, 9245–9265. https://doi.org/10.1029/2018JC014017

688 Uchiyama, Y., Sengo, N., Kurosawa, K. and Nakayama, A., 2018c. Development of a coupled HYCOM-
689 ROMS downscaling ocean modeling system and its application to the South China Sea, Proc.
690 13th International Conference on Hydrodynamics (ICHD2018), pp. 358–363.

691 Uchiyama, Y., Takaura, N., Okada, N., Nakayama, A. 2019. Residual circulations and associated water
692 mass transport in the South China sea analyzed with a coupled HYCOM-ROMS downscaling
693 ocean model. AIP Conference Proceedings 2157, 020029. https://doi.org/10.1063/1.5126564

694 Uchiyama, Y., Tokunaga, N., Aduma, K., Kamidaira, Y., Tsumune, D., Iwasaki, T., Yamada, M., Tateda,
695 Y., Ishimaru, T., Ito, Y., Watanabe, Y.W., Ikehara, K., Fukuda, M. and Onda, Y., 2021. A storm-
696 induced flood and associated nearshore dispersal of the river-derived suspended ^{137}Cs, Sci. Total
697 Environ., 816, 151573, https://doi.org/10.1016/j.scitotenv.2021.151573

698 van Sebille, E., Delandmeter, P., Schofield, J., Hardesty, B.D., Jones, J., Donnellly, D., 2019. Basin-
699 scale sources and pathways of microplastic that ends up in the Galápagos Archipelago. Ocean.
700 Sci. 15, 1341–1349. https://doi.org/10.5194/os-15-1341-2019

701 van Sebille, E., Aliani, S., Law, K.L., Maximenko, N., Alsina, J.M., Bagaev, A., Bergmann, M., Chapron,
702 B., Chubarenko, I., C´ozar, A., Delandmeter, P., Egger, M., Fox-Kemper, B., Garaba, S.P.,
703 Goddijn-Murphy, L., Hardesty, B.D., Hoffman, M.J., Isobe, A., Jongedijk, C.E., Kaandorp, M.L.
704 A., Khatmullina, L., Koelmans, A.A., Kukulka, T., Laufkötter, C., Lebreton, L., Lobelle, D., Maes,
705 C., Martinez-Vicente, V., Maqueda, M.A.M., Poulain-Zarcos, M., Rodríguez, E., Ryan, P.G.,
706 Shanks, A.L., Shim, W.J., Suaria, G., Thiel, M., van den Bremer, T.S., Wichmann, D., 2020. The
707 physical oceanography of the transport of floating marine debris. Environ. Res. Lett. 15, 023003.
708 https://doi.org/10.1088/1748-9326/ab6d7d

Yi, K., Zhang, J., Qian, P.Y., Jian, W., Huang, L., Chen, J., Wu, M.C.S., 2004. Effect of wind events on phytoplankton blooms in the Pearl River estuary during summer. Continental Shelf Research. 24, 1909–1923. https://doi.org/10.1016/j.csr.2004.06.015

Woodall, L.C., Sanchez-Vidal, A., Canals, M., Paterson, G.L., Coppock, R., Sleight, V., Calafat, A., Rogers, A.D., Narayanaswamy, B.E., Thompson, R.C., 2014. The deep sea is a major sink for microplastic debris. R. Soc. Open Sci. 1, 140317. https://doi.org/10.1098/rsos.140317

Wyrtki K., 1961. Scientific results of marine investigations of the South China Sea and the Gulf of Thailand 1959–1961, Naga Report 2, Technical Report, Scripps Institute of Oceanography. 195 pp.

Zhang, X., Uchiyama, Y. and Nakayama, A., 2019. On relaxation of the influences of treated sewage effluent on an adjacent seaweed farm in a tidal strait, Mar. Pollut. Bull., 144, 265-274. https://doi.org/10.1016/j.marpolbul.2019.04.050

Zhang, Z., Wu, H., Peng, G., Xu, P., Li, D., 2020. Coastal ocean dynamics reduce the export of microplastics to the open ocean. Sci. Total Environ. 713, 136634. https://doi.org/10.1016/j.scitotenv.2020.136634

Zhu, L., Wang, H., Chen, B., Sun, X., Qu, K., Xia, B., 2019a. Microplastic ingestion in deep-sea fish from the South China Sea. Sci. Total Environ. 677, 493-501. https://doi.org/10.1016/j.scitotenv.2019.04.380

Zhu, Y., Sun, J., Wang, Y., Li, S., Xu, T., Wei, Z., Qu, T., 2019b. Overview of the multi-layer circulation in the South China Sea. Progress in Oceanography. 175, 171-182. https://doi.org/10.1016/j.pocean.2019.04.001